

# Interface states of rectangular photonic crystals with dislocated and non-dislocated photonic bandgaps

Jianzhi Chen, Jianlan Xie, Exian Liu, Bei Yan, and Jianjun Liu\*

*Key Laboratory for Micro/Nano Optoelectronic Devices of Ministry of Education & Hunan Provincial Key Laboratory of Low-Dimensional Structural Physics and Devices, School of Physics and Electronics, Hunan University, Changsha 410082, China*

\*Corresponding author: [jianjun.liu@hnu.edu.cn](mailto:jianjun.liu@hnu.edu.cn)

**Abstract:** In this paper, the interface with two 2D photonic crystals (PCs) is constructed with different rectangular lattices but the same material, shape and size of dielectric rods and interface states are realized. The existence of interface states is analyzed with Zak phase and surface impedance. When the length-width ratio of rectangular lattices is changed, the retainabilities of the interface states with dislocated and non-dislocated photonic bandgaps (PBGs) are studied by the relationship between length-width ratio of rectangular lattice and Zak phase. It is found that, when the interface states are realized by changing the length-width ratio of rectangular lattices, the retainability of the interface states with dislocated PBGs is mainly influenced by the positions of PBGs, while the retainability of the interface states with non-dislocated PBGs is mainly influenced by Zak phases of the bands. At the selected  $k_y$  in this paper, the retainability of the interface states with dislocated PBGs is better than that with non-dislocated PBGs, and it is adjustable. Further study shows that these conclusions are universal applicable to rectangular PCs with different materials, shapes and sizes of dielectric rods. These results provide a new way to realize interface states with only one kind of dielectric rod easily and construct optical waveguide with strong retainability.

## 1. Introduction

PCs are artificially arranged periodic [1,2] or quasi-periodic [3] structure materials with different permittivities. Due to the properties of the photonic bandgap (PBG), photonic localization, negative refraction, etc., PCs can be used for many purposes, such as optical fibers [4–14], lenses [15–24], prisms [25,26], sensors [11,13,27–29], lasers [30–32], filters [8,33], one-way waveguides [34–36], logic gates [37], etc., wherein waveguides are the primary elements of integrated optics [38], which can control the direction of light propagation.

PC waveguide (PCW) can control the light propagation at the specific frequency with the PBG property and waveguide mode [39,40]. The transmission loss of the PCW is low [41]. The interface states in PCs can be used for photonic localization and surface mode coupling [42–49] to control the light propagation and realize the waveguide effect. Nearly 100% transmission can be achieved by the bend waveguide with interface states [50], and the other special properties of interface states have

attracted the attention of the researchers as that, the existence of interface states is related to PBGs, surface impedances and Zak phases of the two PCs [51–60]; due to topological protection, interface states can exist between two PCs with different topological properties [61–63], while Zak phase is an important topological property [52–59]. The topological properties [64,65] enrich the use of PCs, which will be explained below. The methods commonly used to realize interface states in PCs include band inversion [54–56], structure inversion [57,58] and unit cell translation [59]. In PCs, because of the decisive effect of lattice on bands, the change of lattice structure is bound to directly affect the realization and properties of interface states. Previous researches on interface states of PCs were mainly based on square lattice [54–59], honeycomb lattice [54] or triangular lattice [57] PCs and mostly on square lattice PCs. Since square lattice is just a special case of rectangular lattice, in order to obtain the more universal characteristics of interface states, it is necessary to study the characteristics of interface states in rectangular lattice PCs furtherly. In addition, according to the previous works on interface states in PCs, the materials [54–58], the shapes [57,59] and the sizes [54–57] of scatterers of the two PCs constructing the interface are different, increasing the difficulty of preparation and popularization. Therefore, it is meaningful to find a method to realize interface states with the same dielectric rods on both sides of the interface.

In order to find a method to optimize the effect of interface states with rectangular lattice, the methods to realize interface states can be categorized as dislocated PBGs and non-dislocated PBGs, and a comparative study of them should be made. For dislocated PBGs, the  $m^{\text{th}}$  PBG of  $\text{PC}_1$  and the  $n^{\text{th}}$  PBG of  $\text{PC}_2$  overlap each other on frequency when  $m \neq n$ , while for non-dislocated PBGs,  $m = n$ . By summarizing the previous works, it can be found that, if the interface states are realized by band inversion [54–56], the interface states are usually realized under the premise of dislocated PBGs, however, this method requires the establishment of Dirac point first, that is, a strict selection of materials and structures is required. If the interface states are realized by structure inversion [57,58], due to the limitation of the relationship between geometric and band structures, the interface states are generally realized under the premise of non-dislocated PBGs. When it comes to unit cell translation [59], the realization of the interface states must be based on the premise of non-dislocated PBGs. When the length-width ratio of rectangular lattice is taken as the only variant to study the influence of it on interface states, although it is different from the previous methods, it is still possible to realize interface states in a certain rule, while there should be obvious differences in the difficulty and effect of realizing interface states with dislocated PBGs and non-dislocated PBGs. Therefore, the study and comparison of the interface states with dislocated PBGs and non-dislocated PBGs can provide a new method for realizing interface states and optimizing the characteristics.

In this paper, the interface is constructed with different rectangular lattices and the same material, shape and size of the dielectric rods of the two PCs realizing interface states more easily because of the same dielectric rods, and the interface states are realized with dislocated PBGs and non-dislocated PBGs, then it is found that the retainability of the interface states with dislocated PBGs is mainly influenced by the

positions of PBGs, while the retainability of the interface states with non-dislocated PBGs is mainly influenced by Zak phases of the bands. Moreover, it is found that the existence of the interface states with dislocated PBGs is not easily affected by the change of rectangle lattice at the selected  $k_y$  in this paper, and it is adjustable. The same conclusions can be obtained by changing the material, the shape and the size of the dielectric rods.

## 2. Model and theory

In this paper, the PCW model for realizing interface states is shown in Fig. 1. The waveguide structure consists of two semi-infinite rectangular lattice PCs. The radii of the circular dielectric rods of the two PCs are  $r = 0.2\mu\text{m}$ , and the materials of the rods are all silicon with relative permittivity  $\epsilon_r = 11.9$ , while the background material is air. The lattice constants of the two PCs are set as  $a_x = a = 1\mu\text{m}$  in the  $x$  direction, and  $a_{y1}$  and  $a_{y2}$  (both called as  $a_y$  as the case may be) in the  $y$  direction respectively. The ratio of the lattice constants in the two directions is defined as the length-width ratio of the rectangular lattice  $\eta = a_y/a_x$ . In this paper, by changing  $a_{y1}$  and  $a_{y2}$ , in other words, by changing the length-width ratios of the rectangular lattices of the two PCs, generation and properties of interface states are studied. In the specific simulation calculation below, the numbers of dielectric rods along the  $x$  direction in the region of  $\text{PC}_1$  and  $\text{PC}_2$  are both 5, and the point light source is set below at the  $y$  axis (as shown as the red arrow).

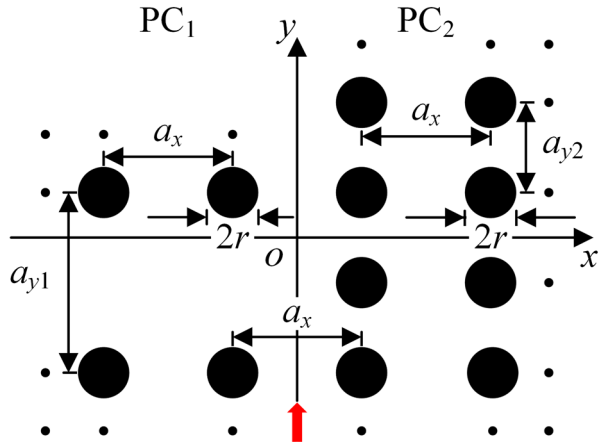


**Fig. 1.** The PCW model for realizing interface states along  $y$  axis.

For the convenience of research, the band of interface states is calculated by selecting  $a_{y1} = 2a_{y2}$  firstly. If  $a_{y1} = 1.4\mu\text{m}$  ( $\eta_1 = 1.4$ ),  $a_{y2} = 0.7\mu\text{m}$  ( $\eta_2 = 0.7$ ), the projected band structures for TM polarization of the two PCs and the eigenfield distribution are shown in Fig. 2.

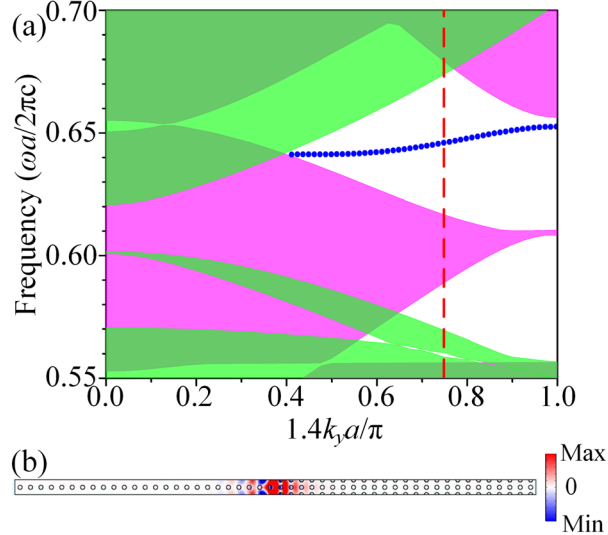


**Fig. 2.** (a) The projected band structures of the two PCs. The pink regions represent the passing bands of  $PC_1$  while the light green regions represent the passing bands of  $PC_2$ , and the dark green regions represent the common bands of the two PCs; (b) the eigenfield distribution of an interface state with  $f = 0.6457c/a$  at  $k_y = 3\pi/(5.6a)$  (indicated by the red dashed line in (a)) in the projected band structures.

In Fig. 2(a), the interface states appear at the common PBG as shown as the band indicated by the blue dotted line. As shown in Fig. 2(b), the eigenfield distribution is localized at the interface of the two PCs.

For the 2D PCs, the necessary condition to realize an interface state is that at a specific  $k_y$  (that is, in a 1D system) and frequency, the sum of surface impedances ( $Z$ ) on both sides of the interface is 0 [66–68]. Within the range of PBG, the real part of surface impedance of PC is 0, and only the imaginary part of surface impedance ( $Im(Z)$ ) affects how the wave reflects and propagates at the interface, that is to say, it is enough that only the sum of the imaginary parts of the surface impedances is 0 to realize an interface state, so

$$Im(Z_1) + Im(Z_2) = 0, \quad (1)$$

where  $Z_1$  ( $Z_2$ ) is the surface impedance of the left (right) side semi-infinite PC at a specific  $k_y$  and frequency. In 1D system (e.g., 1D PC, and 2D PC at a specific  $k$ ) with mirror symmetry,  $Im(Z)$  of the adjacent PBGs (we define the  $(n-1)^{th}$  gap as  $gap(n-1)$  and the  $n^{th}$  gap as  $gap(n)$ ) have the following relationship [55–59] with the Zak phase ( $\varphi$ ) of the  $(n-1)^{th}$  band:

$$\frac{sgn[Im(Z_{gap(n)})]}{sgn[Im(Z_{gap(n-1)})]} = -\exp(i\varphi_{n-1}). \quad (2)$$

By Eq. (2), the sign of  $Im(Z)$  can be figured out with Zak phase ( $\varphi$ ), and then the existence of interface states can be analyzed with Eq. (1). Referring to the method of calculation of Zak phase of 1D system, the projected band structures along the  $k_x$

direction at  $k_y = 3\pi/(5.6a)$ , eigenfield distributions and Zak phases of the two PCs are shown in Fig. 3.

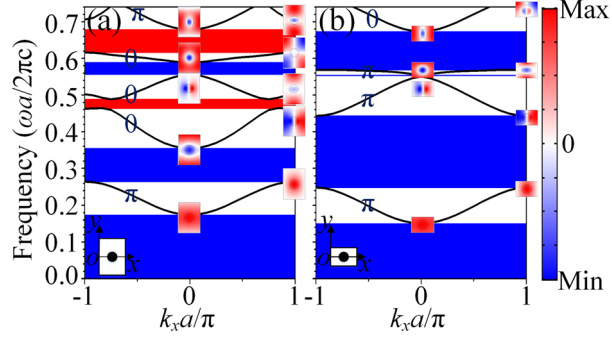


**Fig. 3.** The projected band structures along the  $k_x$  direction at  $k_y = 3\pi/(5.6a)$ , eigenfield distributions and Zak phases of the two PCs: (a) PC<sub>1</sub>; (b) PC<sub>2</sub>. The colors of the PBGs represent the signs of  $\text{Im}(Z)$  with red for positive and blue for negative. The coordinates for calculating surface impedance and Zak phase are shown in the lower left corner of the subfigures, and the origins are in the center of the left boundary of the cells.

The coordinate system is established in the cell, and the origin is chosen at the edge of the cell because surface impedance and Zak phase are calculated at the edge of the cell [60]. Considering the symmetry of the eigenvalues of the two high symmetric points in the reduced 1D Brillouin zone, Zak phase of each band can be obtained, when the two high symmetric points are  $k_x = -\pi/a$  (labeled by A) and  $k_x = 0$  (labeled by B). According to Kohn's results [69], Zak phase is  $\pi$  if one of  $|\tilde{E}_A(x=0)|$  and  $|\tilde{E}_B(x=0)|$  is 0 and the other is not 0, while Zak phase is 0 if both are 0 or neither.

Therefore, according to the eigenfield distribution, Zak phase corresponding to each band can be obtained, as shown in Figs. 3(a) and 3(b). Here,

$$\tilde{E}_{\bar{k}}(x=0) = \frac{1}{a_y} \int_0^{a_y} E_{\bar{k}}(0, y) e^{-ik_y y} dy, \text{ where } \bar{k} \text{ is relative to point A or B. Due to the}$$

fact that  $\text{Im}(Z)$  of the lowest PBG is always negative [55], according to Eq. (2), the sign of  $\text{Im}(Z)$  in each PBG can be obtained, as shown in Figs. 3(a) and 3(b). When  $f \in [0.6165c/a, 0.6734c/a]$ ,  $\text{Im}(Z_1) > 0$ ,  $\text{Im}(Z_2) < 0$  (where the fifth PBG of PC<sub>1</sub> and the fourth PBG of PC<sub>2</sub> overlap each other). In the range of PBG, as the frequency increases,  $\text{Im}(Z)$  decreases from  $+\infty$  to 0 when  $\text{Im}(Z) > 0$ , while  $\text{Im}(Z)$  decreases from 0 to  $-\infty$  when  $\text{Im}(Z) < 0$  [55]. Therefore, there is a frequency that can make  $\text{Im}(Z_1)$  and  $\text{Im}(Z_2)$  satisfies Eq. (1) within the frequency range that the two PBGs overlap each other, that is, an interface state exists at the interface of the two PCs at this frequency [56]. According to the definition in the **Introduction**, the interface state here is realized with dislocated PBGs.

### 3. Results and discussions

The field distributions of the realized interface states at  $f = 0.6457c/a$  and  $0.6510c/a$  selected from Fig. 2(a) are shown in Fig. 4. Interface states can be observed, and the electric fields are localized at the interface of the two PCs.

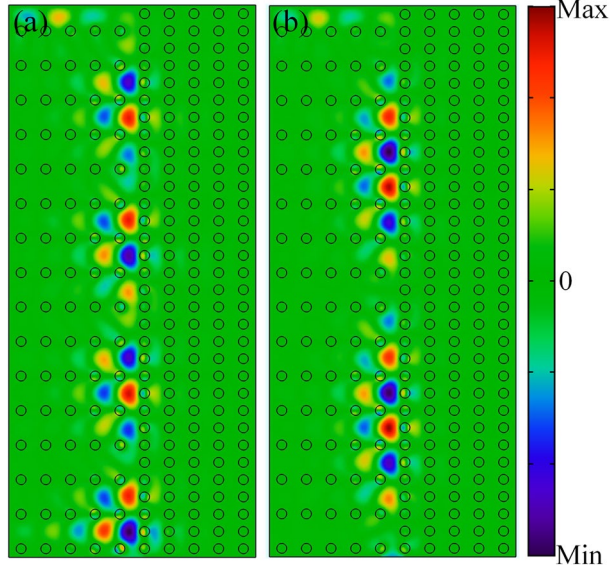


**Fig. 4.** The electric field distributions of two realized interface states: (a)  $f = 0.6457c/a$ ; (b)  $f = 0.6510c/a$ .

In order to furtherly explore the influence of rectangular lattice PCs on interface states, the length-width ratio ( $\eta_2$ ) of rectangular lattice of  $PC_2$  is changed below, while the retainability of interface states is studied under the premise of realizing interface states with dislocated PBGs at  $k_y = 3\pi/(5.6a)$ , and Zak phase and surface impedance are analyzed. The results are shown in Fig. 5.

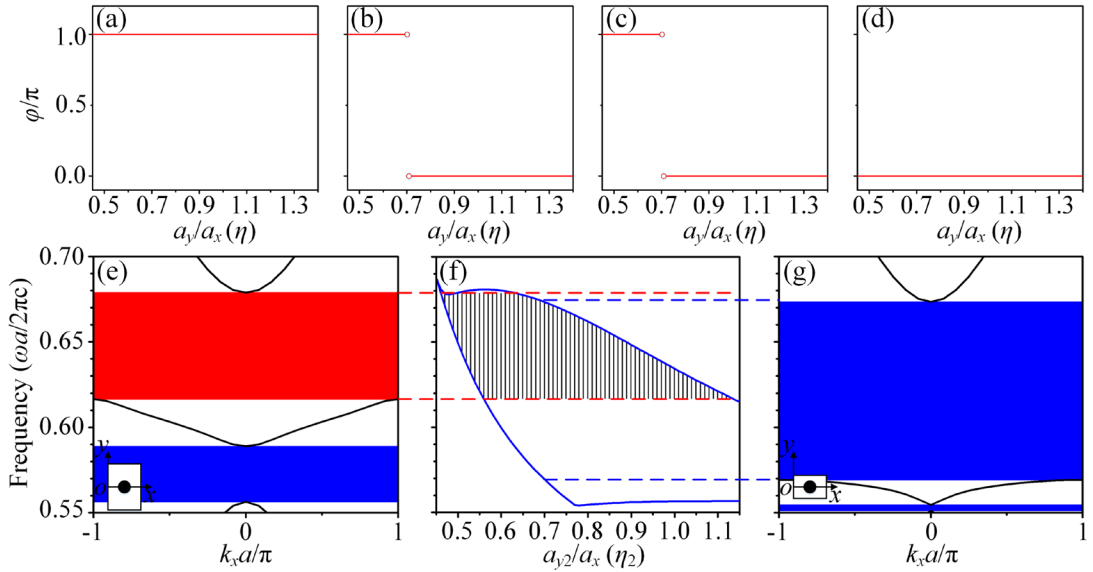


**Fig. 5.** (a)-(d) When  $k_y = 3\pi/(5.6a)$ ,  $a_y \in [0.45a, 1.4a]$ , the changing situation of Zak phase in each band: (a) the first band; (b) the second band; (c) the third band; (d) the fourth band; (e) when  $a_{y1} = 1.4a$ ,  $k_y = 3\pi/(5.6a)$ , the projected band structures intercepted from Fig. 3(a) along the  $k_x$  direction; (f) when  $a_{y1} = 1.4a$ ,  $a_{y2} \in [0.45a, 1.15a]$ ,  $k_y = 3\pi/(5.6a)$ , the schematic diagram of analysis of the

frequency range of corresponding PBGs of interface states realized by the two PCs. The region surrounded by red dashed lines represents the frequency range of the fifth PBG of  $PC_1$ ,  $\text{Im}(Z_1) > 0$ ; the region surrounded by blue solid lines represents the frequency range of the fourth PBG of  $PC_2$  with changing  $a_{y2}$ ,  $\text{Im}(Z_2) < 0$ , and where the ends of the blue dashed lines mark are  $a_{y2}/a_x = 0.7$ ; the region of black vertical lines represents the region of  $\text{Im}(Z_1) > 0$  and  $\text{Im}(Z_2) < 0$  when  $a_{y1}$  is fixed and  $a_{y2}$  is changed, where a certain frequency which can be obtained by the method of Fig. 2(a) exists in any vertical line can satisfy Eq. (1); (g) when  $a_{y2} = 0.7a$ ,  $k_y = 3\pi/(5.6a)$ , the projected band structures intercepted from Fig. 3(b) along the  $k_x$  direction.

According to Eq. (2), surface impedance is correlated with Zak phase, and interface states can be analyzed with Zak phases. As shown in Figs. 5(a)-5(d), when  $k_y = 3\pi/(5.6a)$  and  $a_y \in [0.45a, 0.705a]$ , Zak phases of the second and the third bands are  $\pi$ , and when  $a_y \in (0.705a, 1.4a]$ , Zak phases of the second and the third bands are 0 (that is, the second and the third bands are inverted when  $a_y = 0.705a$ ), while Zak phase of the first (fourth) band is always  $\pi$  (0). According to Eq. (2), although Zak phases of the second and the third bands change as  $a_y$  changes as shown in Figs. 5(b) and 5(c),  $\text{Im}(Z)$  of the fourth PBG is still negative, and  $\text{Im}(Z)$  of the fifth PBG is still positive, in other words, whether Zak phases of the second and the third bands of  $PC_2$  change have no effect on the generation of interface states. By changing  $a_{y1}$  and  $a_{y2}$ , the positions of PBGs of the PCs on both sides can be adjusted to realize dislocation of the PBGs so that the frequency range of the fifth PBG of  $PC_1$  and the frequency range of the fourth PBG of  $PC_2$  overlap each other, then Eq. (1) is satisfied and interface states can be realized.

According to the above analysis, by adjusting  $a_{y2} \in [0.45a, 1.15a]$  with  $a_{y1} = 1.4a$  fixed, the topological properties of interface states of the PCs and the retainability of interface states of the changeable rectangular lattices (the definition of retainability will be explained below) are studied as shown in Fig. 5(f). The frequency range surrounded by red dashed lines is the frequency range for  $\text{Im}(Z_1) > 0$  in the fifth PBG, and the bands of  $PC_1$  and  $\text{Im}(Z_1)$  are shown in Fig. 5(e). The frequency range surrounded by blue solid lines is the frequency range for  $\text{Im}(Z_2) < 0$  in the fourth PBG with changing  $a_{y2}$ . When  $a_{y2} = 0.7a$  where the ends of the blue dashed lines mark, the bands of  $PC_2$  and  $\text{Im}(Z_2)$  are shown in Fig. 5(g). In the region of vertical lines in Fig. 5(f), when  $a_{y1}$  and  $a_{y2}$  are fixed, there is a frequency in the corresponding vertical line that can satisfy Eq. (1), then an interface state can exist. The situation that interface states can still exist when the length-width ratio of the rectangular lattice of the PC changes greatly is called the retainability of interface states of rectangular lattice PCs (it should be noted that, although interface states can still exist, but the frequencies of the interface states may change), hereinafter referred to as retainability. Because of the retainability, when the frequency of incident light changes, interface states can still be realized by adjusting  $a_{y2}$ . According to Fig. 5(f), at  $k_y = 3\pi/(5.6a)$ ,  $a_{y2} \in (0.460a, 1.136a)$  when interface states are realized with dislocated PBGs.

The interface states above are realized by utilizing the retainability of interface states with dislocated PBGs in changing rectangular lattice PCs. According to the above analysis of Zak phase and surface impedance, by adjusting  $a_y$  to change the corresponding frequency range of each PBG, the third PBGs of  $PC_1$  and  $PC_2$  may be

made to have different signs for  $\text{Im}(Z)$ , whose frequency ranges overlap each other (which belongs to the situation of non-dislocated PBGs), and interface states can be realized within this overlapped frequency range. The situation that  $a_{y1} = 0.9a$  ( $\eta_1 = 0.9$ ),  $a_{y2} = 0.45a$  ( $\eta_2 = 0.45$ ) is studied to explore its feasibility of realizing interface states with non-dislocated PBGs, and the results are shown in Fig. 6.

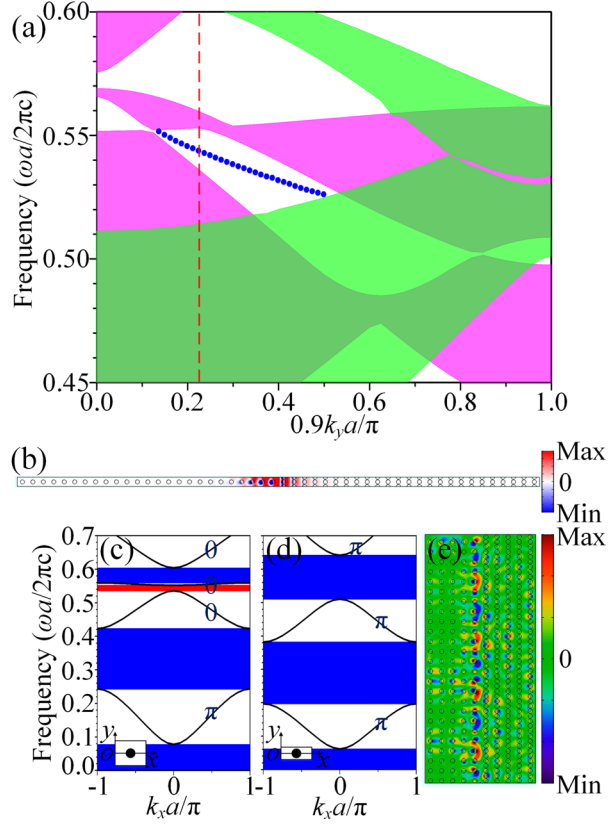


**Fig. 6.** (a) When  $a_{y1} = 0.9a$ ,  $a_{y2} = 0.45a$ , the projected band structures of the two PCs (the red dashed line indicates  $k_y = \pi/(4a)$ ). The pink regions represent the passing bands of PC<sub>1</sub> while the light green regions represent the passing bands of PC<sub>2</sub>. The dark green regions represent the common bands of the two PCs; (b) the eigenfield distribution of an interface state with  $f = 0.5400c/a$  at  $k_y = \pi/(4a)$  (indicated by the red dashed line in (a)) in the projected band structures; the projected band structures along the  $k_x$  direction at  $k_y = \pi/(4a)$  and Zak phases of the two PCs: (c) PC<sub>1</sub>; (d) PC<sub>2</sub>. The colors of the PBGs represent the signs of  $\text{Im}(Z)$  with red for positive and blue for negative. The coordinates for calculating surface impedance and Zak phase are shown in the lower left corner of the subfigures, and the origins are in the center of the left boundary of the cells; (e) the electric field distribution of an realized interface state with  $f = 0.5400c/a$ .

As shown as the blue dotted line in Fig. 6(a), there are interface states in the common PBG. Fig. 6(b) shows the eigenfield distribution with  $f = 0.5400c/a$  at  $k_y = \pi/(4a)$  in the projected band structures, and it can be found that the eigenfield distribution is localized at the interface of the two PCs. According to Figs. 6(c) and 6(d), when  $k_y = \pi/(4a)$ ,  $\text{Im}(Z)$  for the third PBG of PC<sub>1</sub> (PC<sub>2</sub>) is positive (negative), and the PBGs of the two PCs overlaps each other on frequency, then an interface state can be realized in this frequency range, which is consistent with the frequency satisfying Eq. (1) in Fig. 6(a). According to Fig. 6(e), an interface state exists at the

interface of the two PCs with  $f = 0.5400c/a$ . Because the third PBG of  $PC_1$  is narrow so that the distances between the band of interface states and passing bands are small, the effect of photonic localization is not as good as that of the interface states realized with dislocated PBGs.

Similar to Fig. 5, in order to furtherly compare the retainability of the interface states realized with dislocated and non-dislocated PBGs, on the premise of realizing interface states with non-dislocated PBGs, Zak phase and surface impedance are used to study the retainability of the interface states at  $k_y = \pi/(4a)$  by changing the length-width ratio ( $\eta_2$ ) of the rectangular lattice below, and the results are shown in Fig. 7.

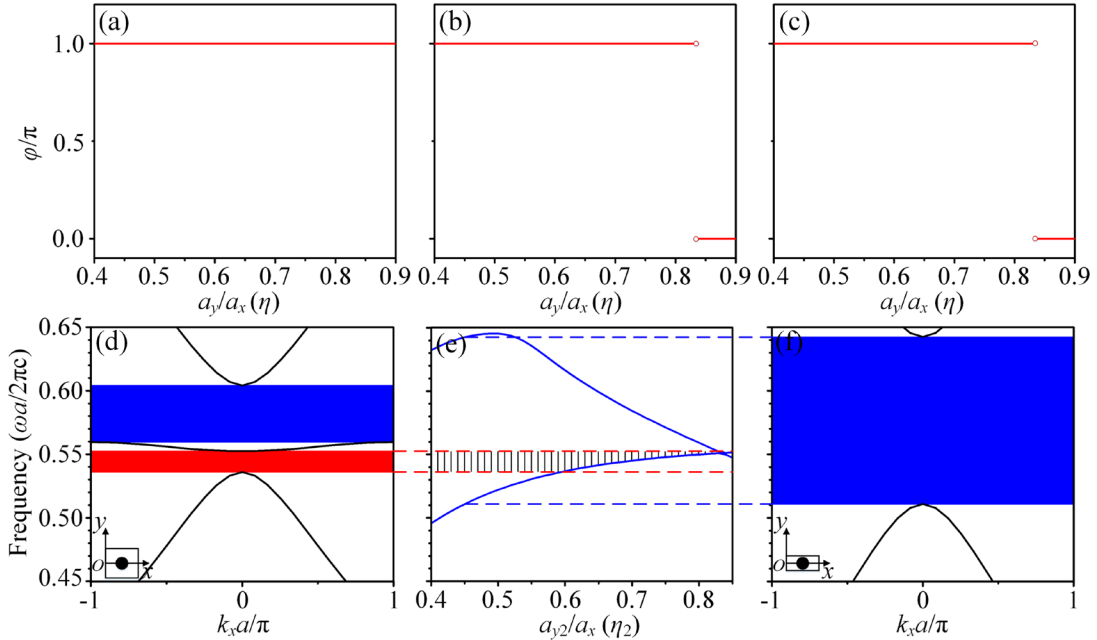


**Fig. 7.** (a)-(c) When  $k_y = \pi/(4a)$ ,  $a_y \in [0.4a, 0.9a]$ , the changing situation of Zak phase in each band: (a) the first band; (b) the second band; (c) the third band; (d) when  $a_{y1} = 0.9a$ ,  $k_y = \pi/(4a)$ , the projected band structures intercepted from Fig. 6(c) along the  $k_x$  direction; (e) when  $a_{y1} = 0.9a$ ,  $a_{y2} \in [0.4a, 0.85a]$ ,  $k_y = \pi/(4a)$ , the schematic diagram of analysis of the frequency range of corresponding PBGs of interface states realized by the two PCs. The region surrounded by red dashed lines represents the frequency range of the third PBG of  $PC_1$ ,  $\text{Im}(Z_1) > 0$ ; the region surrounded by blue solid lines represents the frequency range of the third PBG of  $PC_2$  with changing  $a_{y2}$ ,  $\text{Im}(Z_2) < 0$ , and where the ends of the blue dashed lines mark are  $a_{y2}/a_x = 0.45$ ; the region of black vertical lines represents the region of  $\text{Im}(Z_1) > 0$  and  $\text{Im}(Z_2) < 0$  when  $a_{y1}$  is fixed and  $a_{y2}$  is changed, where a certain frequency (which can be obtained by the method of Fig. 2(a)) exists in any vertical line can satisfy Eq. (1); (f) when  $a_{y2} = 0.45a$ ,  $k_y = \pi/(4a)$ , the projected band structures intercepted from Fig. 6(d) along the  $k_x$  direction.

As shown in Figs. 7(a)-7(c), when  $k_y = \pi/(4a)$  and  $a_y \in [0.4a, 0.835a]$ , Zak phases of the second and the third bands are  $\pi$ , and when  $a_y \in (0.835a, 0.9a]$ , Zak phases of the second and the third bands are 0 (that is, the second and the third bands are inverted when  $a_y = 0.835a$ ), while Zak phase of the first band is always  $\pi$ . According to the above analysis, by adjusting  $a_{y2} \in [0.4a, 0.85a]$  with  $a_{y1} = 0.9a$  fixed, the topological properties of interface states of the PCs and the retainability of interface states of the

changing rectangular lattice are studied as shown in Fig. 7(e). The frequency range surrounded by red dashed lines is the frequency range for  $\text{Im}(Z_1) > 0$  in the third PBG, while the bands of  $\text{PC}_1$  and  $\text{Im}(Z_1)$  are shown in Fig. 7(d). The frequency range surrounded by blue solid lines is the frequency range for  $\text{Im}(Z_2) < 0$  in the third PBG with changing  $a_{y2}$ . When  $a_{y2} = 0.45a$  where the ends of the blue dashed lines mark, the bands of  $\text{PC}_2$  and  $\text{Im}(Z_2)$  are shown in Fig. 7(f). In the region of vertical lines in Fig. 7(e), when  $a_{y1}$  and  $a_{y2}$  are fixed, there is a frequency in the corresponding vertical line that can satisfy Eq. (1), then an interface state can exist, however, due to the narrow PBG, the effect of photonic localization is poor (as shown in Fig. 6(e)). Interface states can be realized (as shown in Fig. 5) whether the second and the third bands of  $\text{PC}_2$  are inverted (that is, whether Zak phases are changed) with dislocated PBGs as long as the fifth PBG of  $\text{PC}_1$  and the fourth PBG of  $\text{PC}_2$  overlap each other on frequency, so its retainability is mainly influenced by the positions of PBGs, while interface states can only be realized when the second and the third bands of  $\text{PC}_2$  are not inverted ( $a_{y2} < 0.835$ ,  $\text{Im}(Z_1) > 0$ ,  $\text{Im}(Z_2) < 0$ ) with non-dislocated PBGs. Interface states cannot be realized once the two bands are inverted ( $a_{y2} > 0.835$ ,  $\text{Im}(Z_1) > 0$ ,  $\text{Im}(Z_2) > 0$ ), so its retainability is mainly influenced by Zak phases of the bands. By comparing Fig. 5(f) with Fig. 7(e), it can be found that  $a_{y2} \in (0.460a, 1.136a)$  (at  $k_y = 3\pi/(5.6a)$ ) when interface states exist with dislocated PBGs, while  $a_{y2} \in [0.4a, 0.835a]$  (at  $k_y = \pi/(4a)$ ) when interface states exist with non-dislocated PBGs, that is, the range of the former is larger than that of the latter, which shows that the interface states with dislocated PBGs has better retainability at the two selected  $k_y$ . It should be emphasized the fact that  $a_{y2} \in [0.4a, 0.835a]$  (at  $k_y = \pi/(4a)$ ) when interface states exist with non-dislocated PBGs is caused by the character of  $\text{PC}_2$  (the second and the third bands are inverted when  $a_y = 0.835a$ , and Zak phases change), while  $a_{y2} \in (0.460a, 1.136a)$  (at  $k_y = 3\pi/(5.6a)$ ) when interface states exist with dislocated PBGs is caused by the character of  $\text{PC}_1$  and  $\text{PC}_2$  (the positions of PBGs), so the range of  $a_{y2}$  can be expanded furtherly when interface states exist with dislocated PBGs by changing the structure of  $\text{PC}_1$  (that is, retainability is adjustable), which also represents an advantage of the interface states with dislocated PBGs.

According to the above analysis, at the selected  $k_y$ , the interface states of the rectangular lattice PCs are more retainable with dislocated PBGs, and this conclusion is related to the relationship between the impedance, the width and the position of PBGs and the lattice constant, that is, the retainability of the interface states depends on the changing rule of Zak phases of the bands and the PBGs with the lattice constant in the rectangular lattice PCs. Further analysis of the characteristics of the interface states of the rectangular PCs with different materials, shapes and sizes of dielectric rods (as shown in [Appendix](#)) shows that this conclusion is universal.

In this paper, based on the two PCs with the same kind of dielectric rods (materials, shapes and sizes are same) and different length-width ratios of rectangular lattices, the changing rule of Zak phases ( $\varphi$ ) of rectangular lattice PCs with the length-width ratio ( $\eta_2$ ) of rectangular lattices is analyzed by fixing the length-width ratio ( $\eta_1$ ) of a rectangular lattice and changing the length-width ratio ( $\eta_2$ ) of the other rectangular lattice, thus the law that interface states are realized by changing the length-width

ratios of rectangular lattices is obtained, which establishes foundation for adjusting the size of lattice to realize the effect for optimizing transmission effect in waveguide under the premise of realizing interface states.

#### 4. Conclusions

Two PCs with different rectangular lattices but the same material, shape and size of dielectric rods on both sides of the interface are constructed to realize interface states easily in this paper, and the mechanism of realizing interface states with Zak phase and surface impedance is analyzed to prove this way to realize interface states is feasible. When interface states are realized with dislocated PBGs and non-dislocated PBGs in rectangular lattice PCs, the retainability of interface states is analyzed with topological property of Zak phase at two selected  $k_y$  when the length-width ratio of the rectangular lattice changes. It is found that the retainability with dislocated PBGs is mainly influenced by the positions of PBGs, while the retainability with non-dislocated PBGs is mainly influenced by Zak phases of the bands, and compared to the interface states with non-dislocated PBGs, the retainability of the interface states with dislocated PBGs is better and adjustable. These conclusions are suitable for the properties of interface states of rectangle lattice PCs with different materials, shapes and sizes of dielectric rods, and provide a new way to construct optical waveguide with strong retainability.

#### Appendix: The characteristics of the interface states of the rectangular PCs with different materials, shapes and sizes of dielectric rods

Suppose the materials of the square dielectric rods of the two PCs are all germanium ( $\varepsilon_r = 16$ ) with a side length  $d = 0.32\mu\text{m}$ . The structures of the combination of the two PCs: Structure 1:  $a_{y1} = 1.4a$  ( $\eta_1 = 1.4$ ),  $a_{y2} = 0.7a$  ( $\eta_2 = 0.7$ ); Structure 2:  $a_{y1} = 0.9a$  ( $\eta_1 = 0.9$ ),  $a_{y2} = 0.45a$  ( $\eta_2 = 0.45$ ). Firstly, we study whether the two structures can respectively realize interface states with dislocated or non-dislocated PBGs, as shown in Fig. 8.

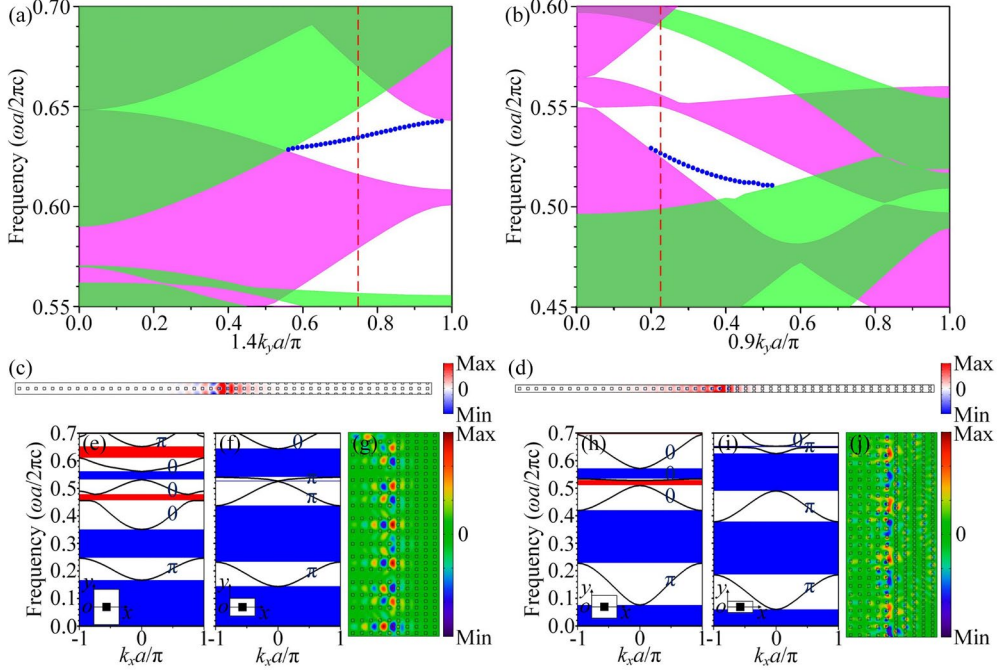


**Fig. 8.** (a), (b) The projected band structures of the PCs in Structures 1 and 2 (the red dashed lines indicate  $k_y = 3\pi/(5.6a)$  and  $\pi/(4a)$  respectively, and the corresponding frequencies of the interface states are  $f = 0.6343c/a$  and  $0.5266c/a$  respectively). The pink regions represent the passing bands of PC<sub>1</sub> while the light green regions represent the passing bands of PC<sub>2</sub>. The dark green regions represent the common bands of the two PCs; (c), (d) the eigenfield distributions of interface states with  $f = 0.6343c/a$  and  $0.5266c/a$  in the projected band structures of Structures 1 and 2; the projected band structures along the  $k_x$  direction at  $k_y = 3\pi/(5.6a)$  and Zak phases of the two PCs in Structure 1: (e) PC<sub>1</sub>; (f) PC<sub>2</sub>; (g) the electric field distribution of an realized interface state with  $f = 0.6343c/a$  in Structure 1; the projected band structures along the  $k_x$  direction at  $k_y = \pi/(4a)$  and Zak phases of the two PCs in Structure 2: (h) PC<sub>1</sub>; (i) PC<sub>2</sub>; (j) the electric field distribution of an realized interface state with  $f = 0.5266c/a$  in Structure 2.

According to Figs. 8(a) and 8(b), both structures can realize interface states. According to Figs. 8(c) and 8(d), both the eigenfield distribution are localized at the interface of the two PCs. Similar to the analysis of surface impedance and Zak phase in Figs. 3, 6(c) and 6(d), in Figs. 8(e) and 8(f), there is a frequency satisfies Eq. (1) in the fifth PBG of PC<sub>1</sub> and the fourth PBG of PC<sub>2</sub> in Structure 1, so an interface state exists with dislocated PBGs [55,56,66–68]. In Fig. 8(g), an interface state exists at the interface between the two PCs of Structure 1 with  $f = 0.6343c/a$ . In Figs. 8(h) and 8(i), there is a frequency satisfies Eq. (1) in the third PBGs of PC<sub>1</sub> and PC<sub>2</sub> in Structure 2, so an interface state exists with non-dislocated PBGs [55,56,66–68]. In Fig. 8(j), an interface state exists at the interface between the two PCs of Structure 2 with  $f = 0.5266c/a$ .

Similar to Figs. 5 and 7, changing the length-width ratio of the rectangular lattice ( $\eta_2$ ) of PC<sub>2</sub>, the retainabilities of the two kinds of interface states are studied with Zak phase and surface impedance with dislocated PBGs (as shown in Fig. 9,  $k_y = 3\pi/(5.6a)$ ) and non-dislocated PBGs (as shown in Fig. 10,  $k_y = \pi/(4a)$ ) to realize interface states.

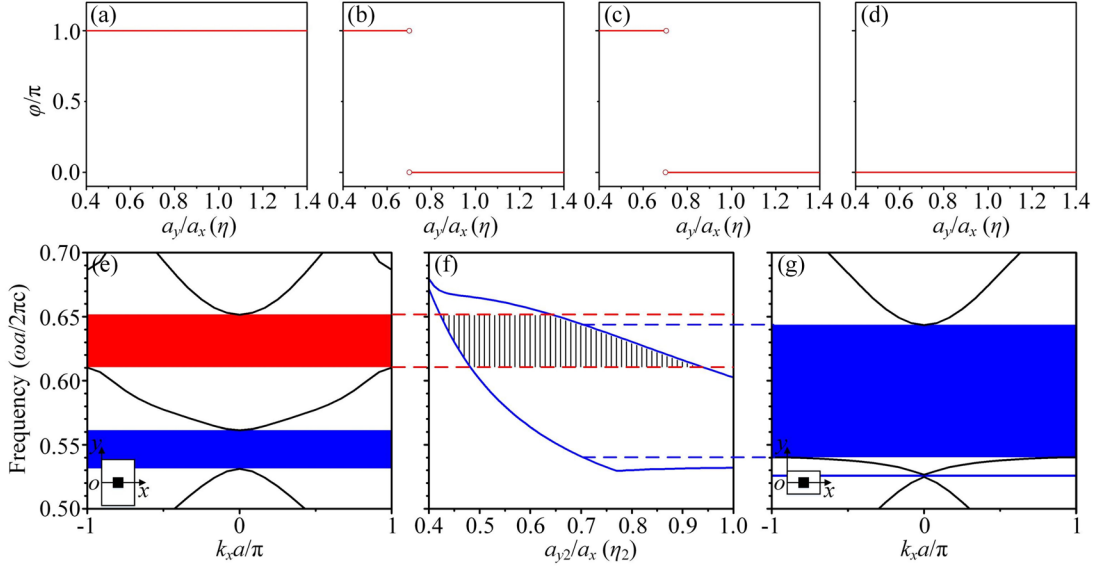


**Fig. 9.** (a)-(d) When  $k_y = 3\pi/(5.6a)$ ,  $a_y \in [0.4a, 1.4a]$ , the changing situation of Zak phase in each band: (a) the first band; (b) the second band; (c) the third band; (d) the fourth band; (e) when  $a_{y1} = 1.4a$ ,  $k_y = 3\pi/(5.6a)$ , the projected band structures intercepted from Fig. 8(e) along the  $k_x$  direction; (f) when  $a_{y1} = 1.4a$ ,  $a_{y2} \in [0.4a, a]$ ,  $k_y = 3\pi/(5.6a)$ , the schematic diagram of analysis of the frequency range of corresponding PBGs of interface states realized by the two PCs. The region surrounded by red dashed lines represents the frequency range of the fifth PBG of  $PC_1$ ,  $Im(Z_1) > 0$ ; the region surrounded by blue solid lines represents the frequency range of the fourth PBG of  $PC_2$  with changing  $a_{y2}$ ,  $Im(Z_2) < 0$ , and where the ends of the blue dashed lines mark are  $a_{y2}/a_x = 0.7$ ; the region of black vertical lines represents the region of  $Im(Z_1) > 0$  and  $Im(Z_2) < 0$  when  $a_{y1}$  is fixed and  $a_{y2}$  is changed, where a certain frequency which can be obtained by the method of Fig. 2(a) exists in any vertical line can satisfy Eq. (1); (g) when  $a_{y2} = 0.7a$ ,  $k_y = 3\pi/(5.6a)$ , the projected band structures intercepted from Fig. 8(f) along the  $k_x$  direction.

As shown in Figs. 9(a)-9(d), when  $k_y = 3\pi/(5.6a)$  and  $a_y \in [0.4a, 0.701a]$ , Zak phases of the second and the third bands are  $\pi$ , and when  $a_y \in (0.701a, 1.4a]$ , Zak phases of the second and the third bands are 0 (that is, the second and the third bands are inverted when  $a_y = 0.701a$ ), while Zak phase of the first (fourth) band is always  $\pi$  (0), which is similar to the change rule in Figs. 5(a)-5(d), so we can analyze the retainability of interface states in the similar way, and the result is shown in Fig. 9(f). The frequency range surrounded by red dashed lines is the frequency range for  $Im(Z_1) > 0$  in the fifth PBG, while the bands of  $PC_1$  and  $Im(Z_1)$  are shown in Fig. 9(e). The frequency range surrounded by blue solid lines is the frequency range for  $Im(Z_2) < 0$  in the fourth PBG with changing  $a_{y2}$ . When  $a_{y2} = 0.7a$  where the ends of the blue dashed lines mark, the bands of  $PC_2$  and  $Im(Z_2)$  are shown in Fig. 9(g). In the region of vertical lines in Fig. 9(f), when  $a_{y1}$  and  $a_{y2}$  are fixed, there is a frequency in the corresponding vertical line that can satisfy Eq. (1), then interface states can exist. According to Fig. 9(f), at  $k_y = 3\pi/(5.6a)$ ,  $a_{y2} \in (0.421a, 0.936a)$  when interface states are realized with dislocated PBGs, and the retainability is mainly influenced by the positions of PBGs.

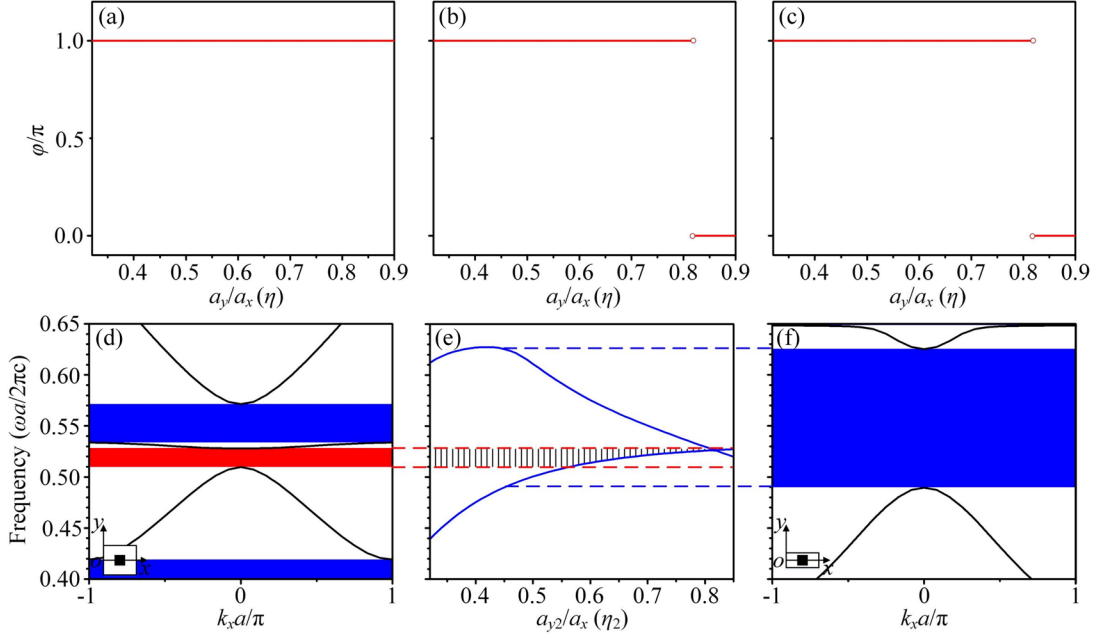


**Fig. 10.** (a)-(c) When  $k_y = \pi/(4a)$ ,  $a_y \in [0.32a, 0.9a]$ , the changing situation of Zak phase in each band: (a) the first band; (b) the second band; (c) the third band; (d) when  $a_{y1} = 0.9a$ ,  $k_y = \pi/(4a)$ , the projected band structures intercepted from Fig. 8(h) along the  $k_x$  direction; (e) when  $a_{y1} = 0.9a$ ,  $a_{y2} \in [0.32a, 0.8a]$ ,  $k_y = \pi/(4a)$ , the schematic diagram of analysis of the frequency range of corresponding PBGs of interface states realized by the two PCs. The region surrounded by red dashed lines represents the frequency range of the third PBG of  $PC_1$ ,  $\text{Im}(Z_1) > 0$ ; the region surrounded by blue solid lines represents the frequency range of the third PBG of  $PC_2$  with changing  $a_{y2}$ ,  $\text{Im}(Z_2) < 0$ , and where the ends of the blue dashed lines mark are  $a_{y2}/a_x = 0.45$ ; the region of black vertical lines represents the region of  $\text{Im}(Z_1) > 0$  and  $\text{Im}(Z_2) < 0$  when  $a_{y1}$  is fixed and  $a_{y2}$  is changed, where a certain frequency which can be obtained by the method of Fig. 2(a) exists in any vertical line can satisfy Eq. (1); (f) when  $a_{y2} = 0.45a$ ,  $k_y = \pi/(4a)$ , the projected band structures intercepted from Fig. 8(i) along the  $k_x$  direction.

As shown in Figs. 10(a)-10(c), when  $k_y = \pi/(4a)$  and  $a_y \in [0.32a, 0.818a]$ , Zak phases of the second and the third bands are  $\pi$ , and when  $a_y \in (0.818a, 0.9a]$ , Zak phases of the second and the third bands are 0 (that is, the second and the third bands are inverted when  $a_y = 0.818a$ ), while Zak phase of the first band is always  $\pi$ , which is similar to the change rule in Figs. 7(a)-7(c), so we can analyze the retainability of interface states in the similar way, and the result is shown in Fig. 10(e). The frequency range surrounded by red dashed lines is the frequency range for  $\text{Im}(Z_1) > 0$  in the third PBG, while the bands of  $PC_1$  and  $\text{Im}(Z_1)$  are shown in Fig. 10(d). The frequency range surrounded by blue solid lines is the frequency range for  $\text{Im}(Z_2) < 0$  in the third PBG with changing  $a_{y2}$ . When  $a_{y2} = 0.45a$  where the ends of the blue dashed lines mark, the bands of  $PC_2$  and  $\text{Im}(Z_2)$  are shown in Fig. 10(f). In the region of vertical lines in Fig. 10(e), when  $a_{y1}$  and  $a_{y2}$  are fixed, there is a frequency in the corresponding vertical line that can satisfy Eq. (1), then interface states can exist. According to Fig. 10(e), at  $k_y = \pi/(4a)$ ,  $a_{y2} \in [0.32a, 0.818a]$  when interface states are realized with non-dislocated PBGs, and the retainability is mainly influenced by Zak phases of the bands.

According to the above analysis, in the case of  $\varepsilon_r = 16$ ,  $d = 0.32\mu\text{m}$ , comparing Fig.

9(f) with Fig. 10(e), it can be found that  $a_{y2} \in (0.421a, 0.936a)$  (at  $k_y = 3\pi/(5.6a)$ ) when interface states exist with dislocated PBGs, while  $a_{y2} \in [0.32a, 0.818a)$  (at  $k_y = \pi/(4a)$ ) when interface states exist with non-dislocated PBGs, that is, the range of the former is larger than that of the latter, which shows that interface states with dislocated PBGs have better retainability at the two selected  $k_y$ . In the same way with the text, the retainability of interface states with dislocated PBGs can be adjusted by changing  $PC_1$ , but the retainability of interface states with non-dislocated PBGs can't be adjusted.

## Funding

National Natural Science Foundation of China (Grant No. 61405058); Natural Science Foundation of Hunan Province (Grant No. 2017JJ2048); Fundamental Research Funds for the Central Universities (Grant No. 531118040112).

## Acknowledgments

The authors acknowledge Prof. Jian-Qiang Liu for software sponsorship.

## Disclosures

The authors declare no conflicts of interest.

## References

1. E. Yablonovitch, “Inhibited spontaneous emission in solid-state physics and electronics,” *Phys. Rev. Lett.* **58**(20), 2059–2062 (1987).
2. S. John, “Strong localization of photons in certain disordered dielectric superlattices,” *Phys. Rev. Lett.* **58**(23), 2486–2489 (1987).
3. Y. S. Chan, C. T. Chan, and Z. Y. Liu, “Photonic band gaps in two dimensional photonic quasicrystals,” *Phys. Rev. Lett.* **80**(5), 956–959 (1998).
4. P. Russell, “Photonic crystal fiber,” *Science* **299**(5605), 358–362 (2003).
5. C. Markos, J. C. Travers, A. Abdolvand, B. J. Eggleton, and O. Bang, “Hybrid photonic-crystal fiber,” *Rev. Mod. Phys.* **89**(4), 045003 (2017).
6. E. Liu, B. Yan, W. Tan, J. Xie, R. Ge, and J. Liu, “Guiding characteristics of sunflower-type fiber,” *Superlattice. Microst.* **115**, 123–129 (2018).
7. E. Liu, W. Tan, B. Yan, J. Xie, R. Ge, and J. Liu, “Broadband ultra-flattened dispersion, ultra-low confinement loss and large effective mode area in an octagonal photonic quasi-crystal fiber,” *J. Opt. Soc. Am. A* **35**(3), 431–436 (2018).
8. B. Yan, A. Wang, E. Liu, W. Tan, J. Xie, R. Ge, and J. Liu, “Polarization filtering in the visible wavelength range using surface plasmon resonance and a sunflower-type photonic quasi-crystal fiber,” *J. Phys. D: Appl. Phys.* **51**(15), 155105 (2018).
9. J. Han, E. Liu, and J. Liu, “Circular gradient-diameter photonic crystal fiber with large mode area and low bending loss,” *J. Opt. Soc. Am. A* **36**(4), 533–539 (2019).
10. E. Liu, S. Liang, and J. Liu, “Double-cladding structure dependence of guiding characteristics in six-fold symmetries photonic quasi-crystal fiber,” *Superlattice. Microst.* **130**, 61–67 (2019).

11. Q. Liu, B. Yan, and J. Liu, "U-shaped photonic quasi-crystal fiber sensor with high sensitivity based on surface plasmon resonance," *Appl. Phys. Express* **12**(5), 052014 (2019).
12. E. Liu, W. Tan, B. Yan, J. Xie, R. Ge, and J. Liu, "Robust transmission of orbital angular momentum mode based on a dual-cladding photonic quasi-crystal fiber," *J. Phys. D: Appl. Phys.* **52**(32), 325110 (2019).
13. C. Li, B. Yan, and J. Liu, "Refractive index sensing characteristics in a D-shaped photonic quasi-crystal fiber sensor based on surface plasmon resonance," *J. Opt. Soc. Am. A* **36**(10), 1663–1668 (2019).
14. Z. Huo, E. Liu, and J. Liu, "Hollow-core photonic quasicrystal fiber with high birefringence and ultra-low nonlinearity," *Chin. Opt. Lett.* **18**, 030603 (2020).
15. Z. Feng, X. Zhang, Y. Wang, Z.-Y. Li, B. Cheng, and D.-Z. Zhang, "Negative refraction and imaging using 12-fold-symmetry quasicrystals," *Phys. Rev. Lett.* **94**(24), 247402 (2005).
16. M. Turduev, E. Bor, and H. Kurt, "Photonic crystal based polarization insensitive flat lens," *J. Phys. D: Appl. Phys.* **50**(27), 275105 (2017).
17. J. Liu and Z. Fan, "Size limits for focusing of two-dimensional photonic quasicrystal lenses," *IEEE Photonic. Tech. L.* **30**(11), 1001–1004 (2018).
18. J. Xie, J. Wang, R. Ge, B. Yan, E. Liu, W. Tan, and J. Liu, "Multiband super-resolution imaging of graded-index photonic crystal flat lens," *J. Phys. D: Appl. Phys.* **51**(20), 205103 (2018).
19. W. Tan, E. Liu, B. Yan, J. Xie, R. Ge, D. Tang, and J. Liu, "Subwavelength focusing of a cylindrically symmetric plano-concave lens based on a one-dimensional Thue-Morse photonic quasicrystal," *Appl. Phys. Express* **11**(9), 092002 (2018).
20. C. Zhang, Z. Jiang, W. Tan, R. Ge, and J. Liu, "Non-near-field sub-diffraction focusing in the visible wavelength range by a Fibonacci subwavelength circular grating," *J. Opt. Soc. Am. A* **35**(11), 1701–1704 (2018).
21. T. Zhou, W. Tan, B. Yan, E. Liu, and J. Liu, "Sub-wavelength focusing in the visible wavelength range realized by a one-dimensional ternary photonic crystal plano-concave lens," *Superlattice. Microst.* **124**, 176–184 (2018).
22. W. Zhang, W. Tan, Q. Yang, T. Zhou, and J. Liu, "Subwavelength focusing in visible light band by a Fibonacci photonic quasi-crystal plano-concave lens," *J. Opt. Soc. Am. B* **35**(10), 2364–2367 (2018).
23. S. Liang, J. Xie, P. Tang, and J. Liu, "Large object distance and super-resolution graded-index photonic crystal flat lens," *Opt. Express* **27**(7), 9601–9609 (2019).
24. Y. Cen, J. Xie, and J. Liu, "Multi-band imaging and focusing of photonic crystal flat lens with scatterer-size gradient," *Chin. Opt. Lett.* **17**(8), 080501 (2019).
25. J. Liu, W. Tan, E. Liu, H. Hu, Z. Fan, T. Zhang, and X. Zhang, "Planar scanning method for detecting refraction characteristics of two-dimensional photonic quasi-crystal wedge-shaped prisms," *J. Opt. Soc. Am. A* **33**(5), 978–983 (2016).
26. J. Upham, B. S. Gao, L. O' Faolain, Z. M. Shi, S. A. Schulz, and R. W. Boyd, "Realization of a flat-band superprism on-chip from parallelogram lattice photonic crystals," *Opt. Lett.* **43**(20), 4981–4984 (2018).

27. R. Ge, J. Xie, B. Yan, E. Liu, W. Tan, and J. Liu, “Refractive index sensor with high sensitivity based on circular photonic crystal,” *J. Opt. Soc. Am. A* **35**(6), 992–997 (2018).

28. Y. Geng, L. Wang, Y. Xu, A. G. Kumar, X. Tan, and X. Li, “Wavelength multiplexing of four-wave mixing based fiber temperature sensor with oil-filled photonic crystal fiber,” *Opt. Express* **26**(21), 27907–27916 (2018).

29. A. Shi, R. Ge, and J. Liu, “Refractive index sensor based on photonic quasi-crystal with concentric ring microcavity,” *Superlattice. Microst.* **133**, 106198 (2019).

30. S. M. Butler, A. P. Bakoz, P. K. J. Singaravelu, A. A. Liles, B. O’ Shaughnessy, E. A. Viktorov, L. O’ Faolain, and S. P. Hegarty, “Frequency modulated hybrid photonic crystal laser by thermal tuning,” *Opt. Express* **27**(8), 11312–11322 (2019).

31. B. H. Le, X. Liu, N. H. Tran, S. Zhao, and Z. Mi, “An electrically injected AlGaN nanowire defect-free photonic crystal ultraviolet laser,” *Opt. Express* **27**(4), 5843–5850 (2019).

32. M. S. Vitiello, M. Nobile, A. Ronzani, A. Tredicucci, F. Castellano, V. Talora, L. H. Li, E. H. Linfield, and A. G. Davies, “Photonic quasi-crystal terahertz lasers,” *Nat. Commun.* **5**, 5884 (2014).

33. Y. -F. Zhao, Z. -M. Wang, Z. -J. Jiang, X. Chen, C. -X. Yue, J. -Z. Wang, and J. -J. Liu, “Add-drop filter with compound structures of photonic crystal and photonic quasicrystal,” *J. Infrared Millim. W.* **36**(3), 342–348 (2017).

34. Z. Wang, K. Su, B. Feng, T. Zhang, W. Huang, W. Cai, W. Xiao, H. Liu, and J. Liu, “Coupling length variation and multi-wavelength demultiplexing in photonic crystal waveguides,” *Chin. Opt. Lett.* **16**(1), 011301 (2018).

35. B. Yan, J. Xie, E. Liu, Y. Peng, R. Ge, J. Liu, and S. Wen, “Topological edge state in the two-dimensional Stampfli-triangle photonic crystals,” *Phys. Rev. Applied* **12**(4), 044004 (2019).

36. T. Hou, R. Ge, W. Tan, and J. Liu, “One-way rotating state of multi-periodicity frequency bands in circular photonic crystal,” *J. Phys. D: Appl. Phys.* **53**(7), 075104 (2020).

37. R. Ge, B. Yan, J. Xie, E. Liu, W. T, and J. Liu, “Logic gates based on edge states in gyromagnetic photonic crystal,” *J. Magn. Magn. Mater.* **500**, 166367 (2020).

38. R. Th. Kersten and W. Rauscher, “A low loss thin-film optical waveguide for integrated optics made by vacuum evaporation,” *Opt. Commun.* **13**(2), 191 (1975).

39. J. G. Maloney, M. P. Kesler, B. L. Shirley, and G. S. Smith, “A simple description for waveguiding in photonic bandgap materials,” *Microw. Opt. Techn. Let.* **14**(5), 261–266 (1997).

40. Y. Tanaka, J. Upham, T. Nagashima, T. Sugiya, T. Asano, and S. Noda, “Dynamic control of the Q factor in a photonic crystal nonacavity,” *Nat. Mater.* **6**, 862–865 (2007).

41. A. Mekis, J. C. Chen, I. Kurland, S. Fan, P. R. Villeneuve, and J. D. Joannopoulos, “High Transmission through Sharp Bends in Photonic Crystal Waveguides,” *Phys. Rev. Lett.* **77**(18), 3787–3790 (1996).

42. D. R. Smith, R. Dalichaouch, N. Kroll, S. Schultz, S. L. McCall, and P. M. Platzman, “Photonic band structure and defects in one and two dimensions,” *J. Opt. Soc. Am. B* **10**(2), 314–321 (1993).

43. W. M. Robertson, G. Arjavalingam, R. D. Meade, K. D. Brommer, A. M. Rappe, and J. D. Joannopoulos, “Observation of surface photons on periodic dielectric arrays,” *Opt. Lett.* **18**(7), 528–530 (1993).

44. Y. T. Fang, X. H. Song, L. Z. Lu, J. J. Wang, Y. X. Jiang and M. Zhu, “Surface waves with near-zero or negative group velocity on one-dimensional photonic crystal coated with one metal film,” *Opt. Commun.* **298**, 129–134 (2013).

45. Y. T. Fang, L. K. Chen, N. Zhu, and J. Zhou, “Tamm states of one-dimensional metal-dielectric photonic crystal,” *IET Optoelectron.* **7**(1), 9–13 (2013).

46. Y. T. Fang, Y. X. Ni, H. Q. He, J. X. Hu. “Effect of hybrid state of surface plasmon–polaritons, magnetic defect mode and optical Tamm state on nonreciprocal propagation,” *Opt. Commun.* **320**, 99–104 (2014).

47. P. A. Kalozoumis, G. Theocharis, V. Achilleos, S. Félix, O. Richoux, and V. Pagneux, “Finite-size effects on topological interface states in one-dimensional scattering systems,” *Phys. Rev. A* **98**(2), 023838 (2018).

48. Y. Zhang, Y. V. Kartashov, and A. Ferrando, “Interface states in polariton topological insulators,” *Phys. Rev. A* **99**(2), 053836 (2019).

49. L. Du, J.-H. Wu, M. Artoni, and G. C. La Rocca, “Phase-dependent topological interface state and spatial adiabatic passage in a generalized Su-Schrieffer-Heeger model,” *Phys. Rev. A* **100**(1), 012112 (2019).

50. S.-Y. Lin, E. Chow, V. Hietala, P. R. Villeneuve, and J. D. Joannopoulos, “Experimental demonstration of guiding and bending of electromagnetic waves in a photonic crystal,” *Science* **282**(5387), 274–276 (1988).

51. D. Agassi and V. Korenman, “Interface states in band-inverted semiconductor heterojunctions,” *Phys. Rev. B* **37**(17), 10095–10106 (1988).

52. J. Zak, “Berry’s phase for energy bands in solids,” *Phys. Rev. Lett.* **62**(23), 2747–2750 (1989).

53. X. Shi, C. Xue, H. Jiang, and H. Chen, “Topological description for gaps of one-dimensional symmetric all-dielectric photonic crystal,” *Opt. Express* **24**(16), 18580–18591 (2016).

54. Z.-Y. Jia, Y.-T. Yang, L.-Y. Ji, and Z.-H. Hang, “Deterministic interface states in photonic crystal with grapheme-allotrope-like complex unit cells,” *Acta Phys. Sin.* **66**(22), 227802 (2017).

55. X. Huang, M. Xiao, Z.-Q. Zhang, and C. T. Chan, “Sufficient condition for the existence of interface states in some two-dimensional photonic crystals,” *Phys. Rev. B* **90**(7), 075423 (2014).

56. Y. Yang, X. Huang, and Z. H. Hang, “Experimental characterization of the deterministic interface states in two-dimensional photonic crystals,” *Phys. Rev. Applied* **5**(3), 034009 (2016).

57. X. Huang, Y. Yang, Z. H. Hang, Z.-Q. Zhang, and C. T. Chan, “Geometric phase induced interface states in mutually inverted two-dimensional photonic crystals,” *Phys. Rev. B* **93**(8), 085415 (2016).

58. X.-D. Chen, D. Zhao, X.-S. Zhu, F.-L. Shi, H. Liu, J.-C. Lu, M. Chen, and J.-W. Dong, “Edge states in self-complementary checkerboard photonic crystals: Zak phase, surface impedance, and experimental verification,” *Phys. Rev. A* **97**(1), 013831 (2018).

59. Y. Yang, T. Xu, Y. F. Xu, and Z. H. Hang, “Zak phase induced multiband waveguide by two-dimensional photonic crystals,” *Opt. Lett.* **42**(16), 3085–3088 (2017).

60. H. Zhang, B. Liu, X. Zhang, Q. Wu, X. Wang, “Zone folding induced tunable topological interface states in one-dimensional phononic crystal plates,” *Phys. Lett. A* **383**(23), 2797–2801 (2019).

61. L. Lu, J. D. Joannopoulos, and M. Soljačić, “Topological photonics,” *Nat. Photon.* **8**, 821–829 (2014).

62. X.-C. Sun, C. He, X.-P. Liu, M.-H. Lu, S.-N. Zhu, and Y.-F. Chen, “Two-dimensional topological photonic systems,” *Prog. Quantum Electron.* **55**, 52–73 (2017).

63. Y. Wu, C. Li, X. Hu, Y. Ao, Y. Zhao, and Q. Gong, “Applications of topological photonics in integrated photonic devices,” *Adv. Opt. Mater.* **5**(18), 1700357 (2017).

64. Y.-L. Xu, L. Feng, M.-H. Lu, and Y.-F. Chen, “Asymmetric optical mode conversion and transmission by breaking PT-symmetry on silicon photonic circuits,” *Phys. Lett. A* **376**(6–7), 886–890 (2012).

65. X. Zhang, H.-X. Wang, Z.-K. Lin, Y. Tian, B. Xie, M.-H. Lu, Y.-F. Chen, and J.-H. Jiang, “Second-order topology and multidimensional topological transitions in sonic crystals,” *Nat. Phys.* **15**, 582–588 (2019).

66. M. Xiao, Z. Zhang, and C. T. Chan, “Surface impedance and bulk band geometric phases in one-dimensional systems,” *Phys. Rev. X* **4**(2), 021017 (2014).

67. M. Xiao, G. Ma, Z. Yang, P. Sheng, Z. Q. Zhang, and C. T. Chan, “Geometric phase and band inversion in periodic acoustic systems,” *Nat. Phys.* **11**, 240 (2015).

68. F. J. Lawrence, L. C. Botten, K. B. Dossou, R. McPhedran, and C. M. de Sterke, “Photonic-crystal surface modes found from impedances,” *Phys. Rev. A* **82**(5), 053840 (2010).

69. W. Kohn, “Analytic properties of bloch waves and wannier functions,” *Phys. Rev.* **115**(4), 809–821 (1959).